# Description and analysis of low-frequency fluctuations in vertical-cavity surface-emitting lasers with isotropic optical feedback by a distant reflector

A. V. Naumenko and N. A. Loiko*
*Institute of Physics, Academy of Sciences of Belarus, Scaryna Prospekt 70, 220072 Minsk, Belarus*

M. Sondermann and T. Ackemann†
*Institute for Applied Physics, University of Münster, Corrensstrasse 2-4, 48149 Münster, Germany*
(Received 14 April 2003; published 12 September 2003)

We analyze theoretically and experimentally the polarization dynamics of vertical-cavity surface-emitting lasers exposed to isotropic optical feedback. The theoretical investigations are based on a model that takes into account different inversion populations for charge carriers with opposite spin. In the deterministic case, we observe toruslike synchronized low-frequency fluctuations of one or both polarization modes in the vicinity of the solitary laser threshold, depending on the parameters and initial conditions. Both in experiment and in simulations including spontaneous emission noise, asymmetric low-frequency fluctuations are observed above and below the solitary laser threshold as well as a transition to coherence collapse further above threshold. The amount of excitation of polarization degrees of freedom and thus the occurrence of simultaneous low-frequency fluctuations of both polarization modes is shown to depend on the magnitude of the dichroism. Apart from the correlation properties on the external-cavity time scale, we find a good qualitative agreement between experiments and simulations.

DOI: 10.1103/PhysRevA.68.033805 PACS number(s): 42.55.Px, 42.60.Mi, 42.65.Sf

## I. INTRODUCTION

Vertical-cavity surface-emitting lasers (VCSELs) are strong competitors to conventional edge-emitting semiconductor lasers for optical communication systems and other applications. Due to their unique geometry, they emit in a single longitudinal mode, have low threshold currents, can be very tightly focused into optical fibers and mass produced in two-dimensional arrays. However, the sensitivity of a VCSEL to optical feedback, which arises inevitably from any surface in the path of the emitted optical beam, is comparable to that of edge-emitting lasers (see, for example, Refs. [1–3]). Moreover, feedback influences not only the amplitude and the phase of the output field but also the polarization state [4–6]. This vulnerability to polarization instabilities is due to the fact that the polarization anisotropy of a VCSEL is only weak because of the circular geometry of its active zone.

Some previous investigations were aimed at using optical feedback to control the polarization dynamics and/or polarization switching. In these investigations, polarization-changing or polarization-selective optical elements were incorporated into the feedback loop. For example, high-frequency polarization modulation was observed in an extended cavity formed by a VCSEL and a partial reflector with a quarter-wave plate inserted between them [6,7]. Polarization-selective feedback is obtained by inserting a linear polarizer in the feedback loop. In that case, switching between orthogonal linearly polarized states is achieved, if the phase of the reflected light is modulated [5,8]. Theoretical investigations of this situation explained the observed phenomena [8,9]. Different kinds of complex behavior arise via the interplay between the intrinsic and external anisotropies [10]. In particular, low-frequency fluctuations (LFF) were demonstrated, which are associated with dropouts in the power of the linearly polarized component of the laser field supported by the polarization-selective feedback and with bursts in the power of the orthogonal component. It was shown that this phenomenon takes place due to the instability of the chaotic ''scalar'' attracting set with respect to orthogonally polarized perturbations in the vicinity of some external-cavity modes belonging to this set. Similar LFF (dropouts in the mode selected by feedback accompanied by intensity bursts in the ''free'' longitudinal modes) were observed in experiments [11] and numerical simulations [12] on edge-emitting lasers.

In this paper we consider theoretically and experimentally the influence of *isotropic* feedback on the dynamics of VCSELs, i.e., the feedback acts equally upon both orthogonally polarized components of the laser field. An important characteristic of the feedback-induced temporal instabilities is that they are often accompanied by *polarization instabilities*, i.e., the particularities related to the vector properties of light are important. A proper understanding of the polarization fluctuations is very important from a practical point of view to control them or to use them in an advantageous way. Differences and similarities to the dynamics of multimode edge-emitting lasers are discussed.

Some aspects of the dynamics in a VCSEL with isotropic optical feedback were studied previously in a limited region of parameters [4,13,14]. In Ref. [4] the existence of LFF and their close connection to polarization dynamics were demonstrated experimentally below the solitary laser threshold. One of the two orthogonal field components was dominant

*FAX: +375-172-840879.
Email address: nloiko@dragon.bas-net.by
†FAX: +49-251-83-33513.

 

and dropouts in its power were accompanied by bursts in the power of the depressed polarization mode. This regime is similar to the regime described above for VCSELs with polarization-selective feedback. However, in the theoretical treatment LFF-like behavior was only found above the solitary laser threshold. A transition to coherence collapse, if the laser is biased above the LFF regime, was predicted theoretically in Ref. [4], but was not found experimentally. Also the connection to the predictions of another theoretical work [14]—appearing simultaneously—was not clear. In the latter paper, simultaneous dropouts in both components were predicted to occur. Recently, experiments yielded the possibility of both scenarios [15]. The important parameter discerning between the different regimes was the amplitude anisotropy (the dichroism) between the two polarization components in the solitary devices. These observations are in qualitative agreement with recent numerical simulations [13]. As a third possibility, LFF behavior was experimentally observed in the dominant polarization component, whereas the orthogonal one stays on the noise level [15].

The aim of this paper is a detailed investigation of the polarization dynamics of VCSELs with feedback in parameter regions matching those used in the experimental investigations. In addition, the investigations cover a wider and/or complementary region of laser parameters compared to Refs. [4,13,14] to elucidate the parameter dependence of the dynamics. Changes in the dynamics due to field contributions from multiple round-trips in the external cavity are also discussed.

For the theoretical studies, we use a model similar to that developed previously for the case of polarization-selective feedback [9]. It is based on the so-called spin-flip model for a solitary VCSEL [16]. It takes into account the dynamics of carrier densities with opposite spin interacting with circularly polarized intracavity fields of specific handiness. In order to describe the effects of feedback, delay terms are added to the field equations. Either a single (i.e., the first) or multiple round-trips in the external cavity are considered. The latter might be important in a VCSEL since the external cavity can have a quite high finesse [4]. Langevin noise terms are used to describe spontaneous emission noise. The model equations and an explanation of the relevant parameters are given in Sec. II.

Section III is devoted to the description of the results obtained by numerical integration of these equations. At first, the deterministic case is considered. The dependence of the dynamics on the feedback level, the pump current and the intrinsic dichroism of VCSEL are elucidated. Different types of LFF at different levels of the pump current and optical feedback are revealed. The influence of spontaneous emission noise on the LFF characteristics is studied in the second part of this section. Experimental results and their comparison with the numerical results are presented in Sec. IV. Section V contains the overall conclusions.

## II. THEORETICAL MODEL

Our model of the polarization dynamics in a quantum well VCSEL with external isotropic feedback starts from the polarization-sensitive rate equations introduced in Ref. [16]. They are modified to include effects of external isotropic feedback. The axes $\hat{x}$, $\hat{y}$ are taken to be parallel (orthogonal, respectively) to the principal axes of the intrinsic amplitude and phase anisotropies, which are assumed to coincide with each other. Then the corresponding equations have the following form:

$$\frac{d}{dt}\overline{E}=\hat{G}\cdot\overline{E}+\overline{F}+\overline{F}_E,$$

$$\frac{d}{dt}\overline{N}=\overline{\mu}+\hat{S}\cdot|\overline{E}|^2-\overline{F}_N, \tag{1}$$

where $N_\pm=N\pm n$, $\gamma=\gamma_a+i\gamma_p$. Column vectors are denoted by "$\overline{\ }$": $\overline{E}\equiv(E_+,\ E_-)$, $|\overline{E}|^2\equiv(|E_+|^2,\ |E_-|^2)$, $\overline{N}\equiv(N,n)$, $\overline{\mu}=(\mu-\Gamma N,-\gamma_s n)$; while matrices are denoted by "$\hat{\ }$":

$$\hat{G}=\begin{pmatrix}\kappa(1+i\alpha)(N_+-1) & -\gamma\\ -\gamma & \kappa(1+i\alpha)(N_--1)\end{pmatrix}$$

and

$$\hat{S}=-\begin{pmatrix}N_+ & N_-\\ N_+ & -N_-\end{pmatrix}.$$

$E_\pm=1/\sqrt{2}(E_x\pm iE_y)$, where $E_x$ and $E_y$ are $\hat{x}$- and $\hat{y}$-polarized components of the slowly varying amplitude of the electromagnetic field; $N$ is the total population difference between the conduction and valence bands; $n$ is the difference of the population differences for the two allowed transitions between magnetic sublevels; $\kappa$ is the mean of the decay rates of the two linearly polarized components of the field; $\alpha$ is the linewidth enhancement factor; $\mu$ is the normalized injection current, which takes the value 1 at the solitary laser threshold; $\gamma_s$ is the decay rate for the difference in the populations of the different magnetic sublevels which results both from spontaneous emission and spin-flip relaxation processes; $\Gamma$ is the decay rate of the total carrier population. We use a typical value of $1/\Gamma\equiv\tau_e=1$ ns. The amplitude and phase anisotropy of the cavity are denoted by the rates $\gamma_a$ and $\gamma_p$. $\gamma_a$ represents the anisotropy in the field decay rate (positive $\gamma_a$ gives the $\hat{y}$-polarized component a lower threshold); $\gamma_p$ represents the linear birefringence of the medium (which gives opposite frequency shifts for the different linearly polarized fields of the solitary laser). Often, $\gamma_a$ is also referred to as *dichroism*.

The feedback $\overline{F}$ from an external mirror taking into account multiple round-trips in the external cavity can be written as

$$\overline{F}(t)=-\varsigma\frac{1}{\tau_{in}}\frac{1-r_2^2}{r_2^2}\sum_{n=1}^{\infty}(-r_2r_3)^n\exp(-i\omega n\tau)\overline{E}(t-n\tau), \tag{2}$$

where $r_2$ and $r_3$ are the amplitude reflectivities of the output VCSEL mirror and the external mirror; $\tau_{in}$ is the round-trip time of the internal (VCSEL) cavity; $\tau$ is the external-cavity round-trip time; $\omega$ is the solitary laser frequency; $\varsigma$ is the coupling factor.

If only one term of sum (2) is considered, the widely used Lang-Kobayashi approximation is recovered [17]. It is valid for such low optical feedback that the field amplitudes resulting from multiple round-trips in the external cavity can be neglected in comparison to the field amplitude of the first round-trip. This condition is satisfied if the quantity $r_2 r_3$ determining the ratio between the field amplitudes of the $(j+1)$th and $j$th round-trips of the external cavity is small enough. Taking into account that the value of $r_2$ is close to unity in a VCSEL, this condition can be easily violated (cf. also Ref. [4]). However, the importance of the contributions of the secondary round-trips might be influenced by effects decreasing the effective coupling strength for an increasing number of round-trips. This might be the limited coherence length of the laser or a decrease in mode overlap due to imperfect mode-matching optics. Hence, we will investigate both cases (single and multiple round-trips) below.

The Langevin noise sources $\overline{F_E} \equiv (F_+, F_-)$ and $\overline{F_N} \equiv (F_N, F_n)$ that arise from spontaneous emission processes have the following form: $\overline{F_\pm} = \sqrt{\beta \Gamma N_\pm}\,\xi_\pm(t)$ and $\overline{F_{(N,n)}} = \Gamma/2\kappa(F_+^* E_+ \pm F_-^* E_- + \text{c.c.})$, where $\beta$ is the spontaneous emission factor (the fraction of the spontaneously emitted photons that go into the lasing modes); and $\xi_\pm$ are two independent complex noise sources with zero mean and correlation $\langle \xi_\pm(t) \xi_\pm^*(t') \rangle = 2\delta(t-t')$. In numerical simulations they are represented as $\xi_\pm(t) = \chi_\pm / \sqrt{\Delta t}$, where $\chi_\pm$ are complex Gaussian random variables (with zero mean and standard deviation $\langle \chi_i \chi_i^* \rangle = 2$), and $\Delta t$ is the time interval over which the noise is held constant.

Steady-state (monochromatic) solutions of systems (1) and (2) in the absence of noise are found in the form $E_\pm = Q_\pm e^{\pm i\psi + i\Omega t}$, $N = N_s$, and $n = n_s$. We present here only linearly polarized states which are divided into two classes polarized along the $\hat{x}$ or along the $\hat{y}$ axis. Their steady-state frequencies are determined from the following transcendent equations:

$$(-\alpha\gamma_a + \gamma_p)(-1)^l + \Omega + \frac{1}{\tau_{in}}[\alpha \,\mathrm{Re}\, f(\Omega) - \mathrm{Im}\, f(\Omega)] = 0, \tag{3}$$

where $l = 0(1)$ corresponds to $\hat{x}$- ($\hat{y}$-)polarized states,

$$f(\Omega) = \varsigma(1-r_2^2)\frac{r_3}{r_2}\frac{\exp i\theta}{1 + r_2 r_3 \exp i\theta},$$

and $\theta = -(\Omega + \omega)\tau$. Equation (3) can be rewritten in the following form:

$$(-\alpha\gamma_a + \gamma_p)(-1)^l + \Omega + \frac{\sigma(\alpha[r_2 r_3 + \cos\theta] - \sin\theta)}{1 + r_2^2 r_3^2 + 2 r_2 r_3 \cos\theta} = 0.$$

The steady inversion

$$N_s = 1 + \frac{1}{k}\left( (-1)^l \gamma_a - \frac{1}{\tau_{in}} \mathrm{Re}\, f(\Omega) \right), \quad n_s = 0,$$

the field amplitudes

$$Q_\pm = \sqrt{\frac{1}{2}\left(\frac{\mu}{N_s} - 1\right)} \quad \text{and} \quad \psi = l\pi/2.$$

The maximum value of the normalized feedback strength $\sigma' = \varsigma(\tau_e/\tau_{in})(1-r_2^2)(r_3/r_2)$ is equal to 120. Below we will use the non-normalized value $\sigma = \sigma'/\tau_e$.

The threshold value of injection current for each steady state is

$$\mu_{th} = 1 + \frac{1}{k}\left( (-1)^l \gamma_a - \frac{1}{\tau_{in}} \mathrm{Re}\, f(\Omega) \right) \quad (\text{or } \mu_{th} = N_s).$$

This results in the following values for the threshold current for $\hat{x}$ ($\hat{y}$) -polarized emission:

$$\mu_{th} = 1 + \frac{1}{k}\left( (-1)^l \gamma_a - \frac{\sigma}{1 + r_2 r_3} \right). \tag{4}$$

The values of basic parameters used in numerical simulations are typical VCSEL parameters or—in the case of the phase and amplitude anisotropies—are taken from experimental measurements: $\kappa = 300\ \mathrm{ns}^{-1}$, $r_2 = 0.9975$, $\tau_{in} = 28$ fs, $\alpha = 5$, $\gamma_s = 20\ \mathrm{ns}^{-1}$, $\gamma_p = 6\pi\ \mathrm{ns}^{-1}$, $\tau = 3$ ns, $\varsigma = 1$, $\Delta t = 10$ ps. The values of the other parameters are varied and are given in the text below. The choice of $\alpha = 5$ is justified in Sec. IV D. The rather low spin-flip rate of $\gamma_s = 20\ \mathrm{ns}^{-1}$ was chosen, since for the devices under study the correlation properties of the two polarization components in the solitary laser could be modeled best by assuming a spin-flip rate of this magnitude [18]. The LFF dynamics with feedback was found to remain qualitatively unchanged for different spin-flip rates in the investigated range from 20 up to 100 $\mathrm{ns}^{-1}$.

## III. NUMERICAL RESULTS

### A. Deterministic dynamics

First, we study the deterministic case when no spontaneous emission noise is considered. The threshold reduction numerically observed is in accordance with Eq. (4).

#### *1. Basic phenomena*

For rather small (positive) values of the dichroism, the solitary VCSEL is bistable near threshold (both linearly polarized components of the laser field are stable with respect to orthogonally polarized perturbations [18,19]). Hence, it is not unexpected that the feedback-induced dynamics depends also on initial conditions: For $\gamma_a = 0.04\pi\ \mathrm{ns}^{-1}$ and biasing the laser at the solitary laser threshold ($\mu = 1$), the system can demonstrate pulsations in the $E_x$ or in the $E_y$ component (correspondingly, the power of the $E_y$ or $E_x$ component tends to zero value with evolving time) or in both field components simultaneously in a wide region of values of feedback strength. An example of the temporal evolution of the $E_x$

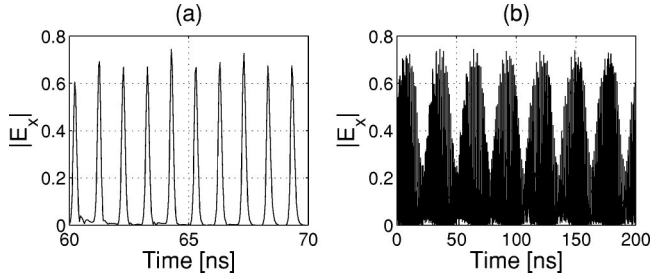


FIG. 1. Time evolution of the field amplitude $|E_x|$ on the short (a) and long (b) time scales, $\gamma_a = 0.04\pi\ \mathrm{ns}^{-1}$, $\sigma = 20\ \mathrm{ns}^{-1}$, $\mu = 1$, $\beta = 0$.

component in the situation when $E_y = 0$ is presented in Fig. 1 for the case of comparatively weak feedback ($\sigma = 20\ \mathrm{ns}^{-1}$). The system displays fluctuations on two time scales. The high-frequency component of these dynamics consists of sharp narrow pulses separated by 1 ns [Fig. 1(a)]. Every third pulse is slightly higher than the others. A main feature of the radio-frequency (rf) spectrum is a comb of equidistant peaks with a frequency separation equal to the external-cavity round-trip frequency of 1/3 GHz (Fig. 2, inset). The most pronounced feature is a peak at 1 GHz (and its harmonics), which is presumingly due to a 1:3 synchronization of the feedback frequency and the relaxation oscillation frequency.

Superimposed on this pulse train is a low-frequency envelope with an average period of about 28 ns [Fig. 1(b)]. This slow modulation has approximately a harmonic shape and is rather regular. As a consequence, there is a narrow, well-defined peak in the rf spectrum at 0.036 GHz (Fig. 2). A detailed analysis shows that the averaged intensity does not reach the zero level in the minima of the low-frequency envelope. In accordance with this, the total population inversion tends to 1 (i.e., the unsaturated value at the solitary laser threshold) in the minima of the averaged intensity, but does not reach this unit value. This dynamical state could be interpreted as a quasiperiodic movement on a torus with two strongly pronounced frequencies: the frequency of the slow modulation and the feedback frequency synchronized with the relaxation oscillation frequency. These features distinguish the observed phenomenon from usual LFF in edge-emitting semiconductor lasers, which are characterized by a

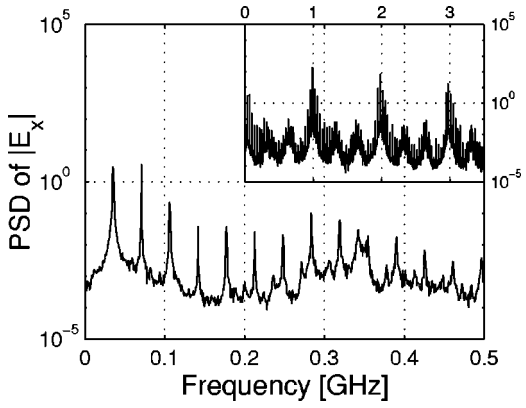


FIG. 2. Rf spectrum corresponding to Fig. 1.

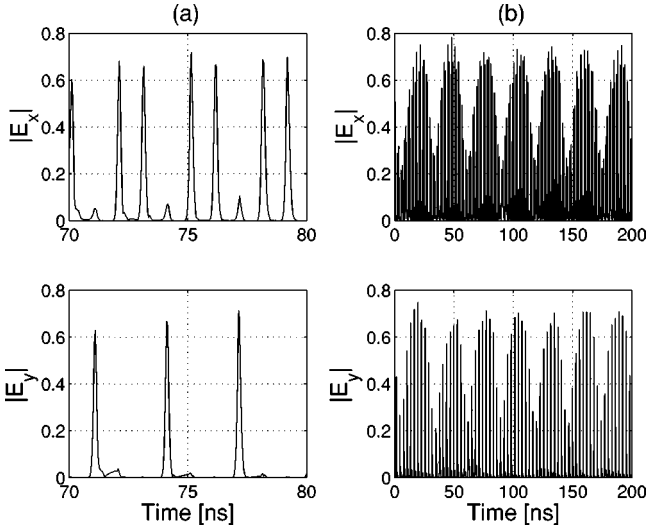


FIG. 3. Time evolution of the field amplitudes $|E_x|$ and $|E_y|$ on the short (a) and long (b) time scales at the same parameters as in Fig. 1 and other initial conditions.

sudden reduction of the laser intensity (dropout) followed by a gradual return to full power [20–22]. However, the obtained behavior is similar to that observed in Refs. [23–25]. It was interpreted as a locking phenomenon, in which the dropout events are synchronized and hence become regular. This goes along with a regular distribution of the sharp intensity pulses during one LFF period. The appearance of this state in a VCSEL model indicates that it is a rather robust and widespread solution of (deterministic) semiconductor laser models with delayed feedback (see also the remarks in Sec IV D).

The toruslike behavior of the *y*-polarized field is also obtained using other initial conditions. However, it is worth noting that the domain of its realization is rather small at weak feedback conditions. The system operates more often on the $E_x$ component though it has a higher threshold in the absence of feedback. Probably, this behavior is connected to the fact that the $E_x$ mode is ''more stable.'' This is in agreement with the fact that in the solitary laser the $E_x$ mode also dominates far enough above the threshold, even if the dichroism (slightly) favors the other mode [18]. For the solitary laser, it is known that this selection is due to the spin dynamics [18,19]. For strong feedback, emission of the loss-favored $E_y$ polarized component is obtained as a rule.

Pulsations in both orthogonal components observed at the same parameters are presented in Fig. 3. Here, the dynamics of the $E_x$ component are similar to that described above. The only difference is a suppression of every third pulse on the fast time scale [Fig. 3(a)]. At these moments, pulses in the $E_y$ component are excited, forming a pulse train with a spacing corresponding to the external-cavity round-trip time of 3 ns. These dominating time scales are clearly evident in the autocorrelation functions of the polarization components [Fig. 4(a)]. The cross-correlation function is close to zero at zero and at 3 ns time lag and shows a correlation at time lags of 1 ns and 2 ns [Fig. 4(b)]. The operating frequencies of the two orthogonal components are approximately separated by $2\gamma_p$.

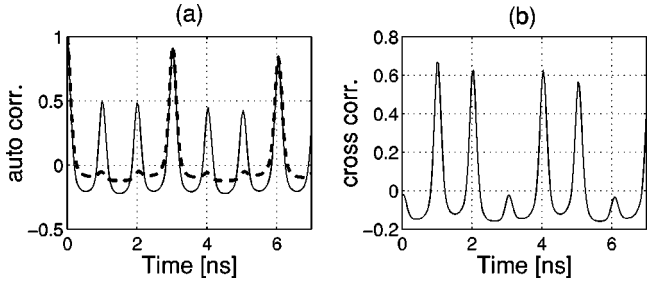


FIG. 4. Autocorrelation functions of $E_x$- (thick line) and $E_y$- (dotted line) field components (a) and their cross-correlation function (b); parameters are the same as in Fig. 3.

Their low-frequency envelopes are correlated [Fig. 3(b)]. Besides this regime, there is a similar one in which the $E_x$ and $E_y$ components exchange the roles.

#### *2. Dependence on feedback level*

We observe a gradual distortion of the torus with increasing feedback level, though the main features are kept up to $\sigma = 100\ \mathrm{ns}^{-1}$. At the same time, the period of the low-frequency component is increased. The quasiperiodic kind of behavior in both polarization components is perturbed earlier than in the case with a single polarization component, if the feedback strength is increased. It disappears for $\sigma > 80 - 90\ \mathrm{ns}^{-1}$. In between—at intermediate feedback level—the simulations yield a kind of ''intermittent'' behavior between the toruslike regime and a regime that resembles ''conventional'' LFF known from edge-emitting lasers [21,22]. An example is shown in Fig. 5. Both field components demonstrate sudden dropouts of the average amplitude, which are followed by recovery processes taking place on slower time scales. This means that the envelope along one LFF event gets an asymmetric shape [Fig. 5(c)] in contrast to the toruslike regime discussed above. Dropout events in the two components occur synchronously. The intensities in the moments of dropouts are very close to a value of zero and the total population inversion reaches approximately the unity value. It is worth noting that synchronous dropouts of individual modes are experimentally observed in multi-longitudinal-mode edge-emitting lasers [26,27] demonstrating again the similarity of the process in both kinds of semiconductor lasers. We would like to emphasize the following difference in the behavior of the two polarization components: Whereas the maximal values of $\langle |E_x| \rangle$ are reached as rule just before the dropouts, the maxima of $\langle |E_y| \rangle$ can be situated between two dropout events [Fig. 5(c)], i.e., the amplitude of the disfavored polarization component can decay before the power buildup in the dominant polarization component (and in the total power) is complete (see also Ref. [4]).

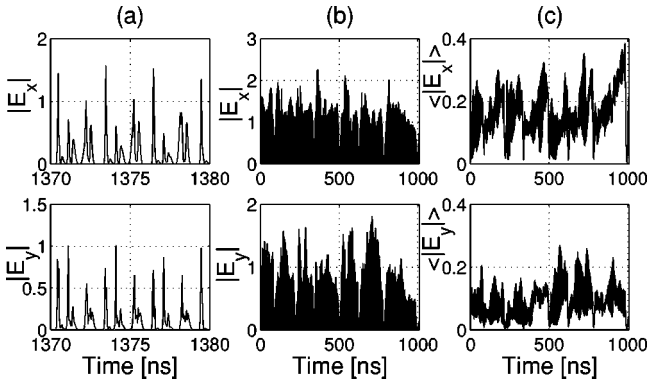


FIG. 5. Time evolution of the field amplitudes $|E_x|$ and $|E_y|$ on the short (a) and long (b) time scales and amplitudes averaged over 1 ns (c), $\sigma = 50\ \mathrm{ns}^{-1}$; other parameters are the same as in Fig. 1.

The average period of this kind of LFF is about three to four times higher than in the case of the toruslike state. For the parameters of Fig. 5, it is about 140 ns. During this period there are evidently some faster modulations [see Fig. 5(b)], which can be interpreted as the remnants of the low-frequency envelope of the torus presented in Fig. 3(b). On the fast time scale, the pulsing in the two orthogonally polarized components occurs also synchronously [Fig. 5(a)]. However, there is anticorrelation regarding the height of the pulses, i.e., a large-amplitude pulse in the $E_x$ component is accompanied by a small-amplitude one in the $E_y$ component and vice versa.

#### *3. Dependence on current, dichroism, and the influence of multiple round-trips*

If the laser is biased above the solitary laser threshold at any feedback level, LFF with sharp dropouts such as those presented in Fig. 5 arise. If the current is increased further, the laser dynamics is transformed into a fully developed coherence-collapse regime, in which the almost-periodic LFF component cannot be identified anymore. The values of the current at which these transformations occur depend on the feedback level: the stronger the feedback, the higher the transition current.

For small negative values of the dichroism, the $E_x$-field component has a lower threshold and is stable with respect to orthogonally polarized perturbations in the solitary laser. In that case, a regime with pulsations in the $E_y$ component and $E_x = 0$ was not obtained in the case with feedback. This behavior can be expected. The other features of the dynamics are similar to those described above. In contrast, for higher positive values of $\gamma_a$ $(0.1\text{–}0.4\pi\ \mathrm{ns}^{-1})$ we observe at the solitary laser threshold perfect selection of the $E_y$ component. The system displays a toruslike regime with 1:4 synchronization of the feedback frequency and the relaxation oscillation frequency.

Both field components are exited only for $\mu > 1$ and the corresponding regime is similar to the LFF presented in Fig. 5. For $\gamma_a = 0.4\pi\ \mathrm{ns}^{-1}$ the $E_x$ component has slightly lesser amplitude than the $E_y$ component (on average).

For $\gamma_a$ between 0.1 and $0.4\pi\ \mathrm{ns}^{-1}$ and moderate feedback strength, the transition point between torus dynamics and LFF coincides approximately with the transition from emission of one polarization mode to emission of both modes. For high dichroism values, the transition from the torus regime to LFF occurs within the range of single-mode operation.

When multiple round-trips in the external cavity are considered, the threshold reduction becomes smaller, which is in

accordance with Eq. (4). The laser dynamics is practically not changed compared to the single-round-trip approximation for considerably weak feedback. The value of $\sigma$ at which the two approximations give different types of behavior depends on the other laser parameters. For the parameters used here ($\gamma_a = 0.1\pi\ \mathrm{ns}^{-1}$, $\mu = 1$), instead of LFF a linearly polarized steady state with $E_x \neq 0$, $E_y = 0$ is obtained in the interval of $\sigma$ 67 $\mathrm{ns}^{-1} < \sigma < 95\ \mathrm{ns}^{-1}$, if $r_3$ is increased. At higher levels of feedback—up to $\sigma \approx 102\ \mathrm{ns}^{-1}$—we observe antiphased pulsations in both polarization components with a weak modulation at the frequency close to that of the torus regime and to the asymmetric LFF frequency. For even higher feedback levels, the system shows LFF with partially antiphased fast dynamics similar to the case described below.

### B. Stochastic dynamics

#### *1. Basic phenomena*

If spontaneous emission noise is included, the character of laser dynamics at the solitary laser threshold ($\mu = 1$) changes drastically compared to the deterministic case.

First, noise results in the stimulation of both linearly polarized field components independently from dichroism and initial conditions. Second, an additional frequency component appears at very low frequencies. Its period is larger than that of the torus by three to four times. (This matches the observations for higher feedback rates in the deterministic case.) For small levels of the noise, this component is only slightly resolved in the dynamics. The corresponding rf spectrum contains a strongly asymmetric component in the low-frequency domain, which is roughly similar to an $1/f$-noise spectrum. Increasing the noise destroys the synchronization of the feedback frequency with the relaxation oscillation frequency on the short time scale. For example, for $\gamma_a = 0.1\pi\ \mathrm{ns}^{-1}$ we observe a more complex structure in the time-interval equal to the feedback delay $\tau$ compared to the four narrow equidistant pulses obtained in the deterministic case [Fig. 6(a)]. The pulses become wider and acquire a kind of internal structure consisting of several closely spaced spikes. The fast oscillations are only approximately repeated with a time lag of $\tau$. The envelope is transformed into asymmetric LFF with sudden dropouts and a rather slow recovery of the laser intensity with an average period of about 117 ns [Fig. 6(b)]. The frequency component corresponding to the movement on the torus on intermediate time scales is almost unresolvable for this level of noise. The spectrum in the low-frequency domain has a rather complex structure with several peaks.

These noise-induced LFF bear many similarities to deterministic LFF obtained for higher feedback levels and/or above the solitary laser threshold described above. The average period of these noise-induced LFF depends only slightly on the level of noise. Their period and the amplitude of oscillations in both polarization components increase for higher values of the feedback strength. The level of noise at which the torus regime is transformed into asymmetric LFF depends on the level of the feedback. (For example, for a weaker feedback rate $\sigma = 20\ \mathrm{ns}^{-1}$, the system shows a torus-like behavior at the same noise level for the parameters of Fig. 6.) These changes in dynamics due to the presence of noise might be interpreted as being due to the amplification or excitation by the noise of an oscillating component already inherent to the system. We conjecture that this might be related to the phenomenon of stochastic resonance [28].

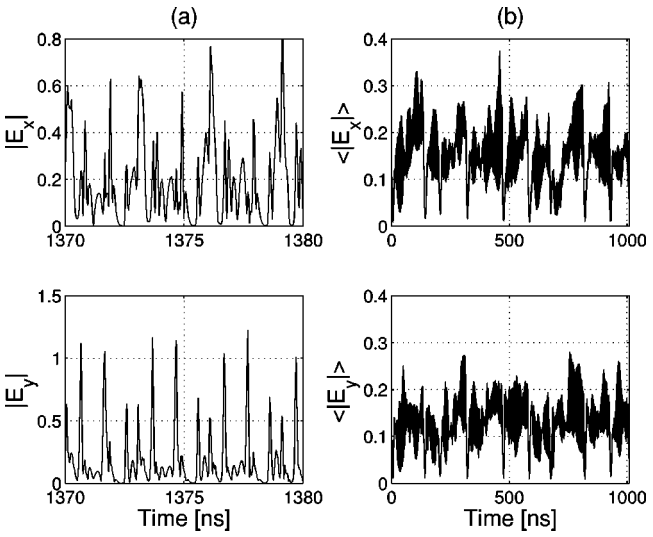


FIG. 6. Time evolution of the field amplitudes $|E_x|$ and $|E_y|$ on the short time scale (a) and amplitudes averaged over 1 ns (b), $\gamma_a = 0.1\pi\ \mathrm{ns}^{-1}$, $\sigma = 50\ \mathrm{ns}^{-1}$, $\mu = 1$, $\beta = 10^{-5}$.

#### *2. Dependence on current*

An increase of the injection current leads to an increase of the frequency of the LFF. This regularity can be considered to be a consequence of the increase of the relaxation oscillations frequency and their damping [29] that determine the time scale of the dynamics.

If the injection current is decreased below the threshold value of the solitary laser, the LFF frequency decreases as expected from the above discussion. Below a certain current value, another regime is observed: oscillations in $E_x$ and $E_y$ components at the short time scale become partly antiphased (Fig. 7). After a dropout event, the amplitudes of both polar-

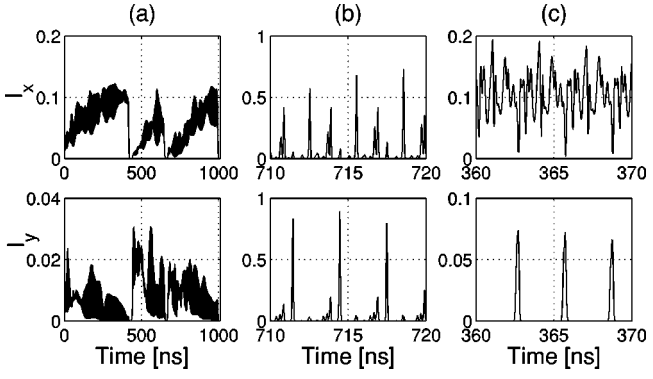


FIG. 7. Intensities $I_x \equiv |E_x|^2$ and $I_y \equiv |E_y|^2$ averaged over 1 ns (a) and on the short time scale (b),(c). Parts (b) and (c) display a short time interval after and before the first dropout event in (a), respectively. $\mu = 0.93$, $\sigma = 50\ \mathrm{ns}^{-1}$; other parameters are the same as in Fig. 6.

ization components oscillate in the same way as for larger values of current, i.e., they show synchronized pulses with strongly alternating amplitudes [Fig. 7(b)]. However, after the recovery process, i.e., before the next dropout event, the character of the oscillations is changed. The dominant component (here $E_x$) shows fluctuations around a nonzero mean together with some more pronounced sharp dips [Fig. 7(c)]. The weaker polarization component (here $E_y$) shows a rather regular train of large-amplitude pulses, which are separated by the cavity round-trip time, and some fluctuations of low amplitude [not visible in Fig. 7(c)]. Both originate from zero intensity level. The high-amplitude pulses in the weak component are accompanied by dips in the strong one. Hence, the total population inversion oscillates within rather small limits.

The evolution of the time-averaged amplitude of the weaker polarization component ($|E_y|$) displays a more pronounced torus component between the dropout events [Fig. 7(a), central event] or shows some decrease already before the dropout [Fig. 7(a), left and right event]. For lower current, the latter behavior becomes more frequent, i.e., a sharp growth of $|E_y|$ occurs just after dropouts and then a slow decrease of the amplitude takes place. This resembles the behavior obtained in Ref. [4] below the solitary laser threshold and more recently in Ref. [13] above the solitary laser threshold.

If the current is decreased further, only the fast antiphased dynamics of $E_x$ and $E_y$ components is observed, without a strong slow modulation. The strength of the anticorrelation increases and the amplitude of the oscillation in the carrier density decreases for decreasing current values. Near the reduced threshold of the laser with feedback, alternation between almost stable $E_y$ emission and antiphased oscillations in both polarization components is found on very long time scales (with a period of about 14 $\mu$s). At this stage, we cannot exclude that this behavior is only a very long transient to periodic oscillations or to the steady state. The transitions between the regimes of stable emission or antiphased oscillations below the solitary laser threshold and the LFF regime around this threshold create kinks in the time-averaged light-current characteristics [light intnsity (LI) curves] characteristics (see also the discussion in Sec. IV B and Fig. 8). An overview of the dynamical regimes observed in the simulations for different injection currents is presented in Fig. 8.

### *3. Spectral properties*

The operating frequencies of the two polarization components (measured in angular frequencies) are separated by $\approx 2\gamma_p$ in the solitary laser [19]. In tendency, this holds also for the laser with feedback in the stochastic as well as in the deterministic case, since the corrections due to optical feedback are similar for both polarization components. The steady-state operating frequencies of the external-cavity modes are determined by Eq. (3). They depend on the feedback level $\sigma$ via $f(\Omega)$. In a dynamical operating condition with multiple external-cavity modes excited, the frequency of the time-averaged line center depends on the mode order of the most excited external-cavity mode and the linewidth or span depends on the number of excited modes. Both are

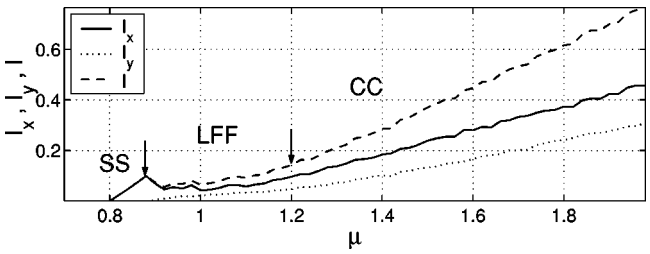


FIG. 8. Polarization resolved (solid line, $|E_x|$ mode; dotted line, $|E_y|$ mode) and total intensity (dashed line) in dependence of the injection current. Parameters are $\gamma_a = 0.04\pi\ \mathrm{ns}^{-1}$, $\sigma = 60\ \mathrm{ns}^{-1}$, other parameters are the same as in Fig. 6. The time-averaged LI curves were calculated by changing the injection current $\mu$ step by step and waiting some time until the transients died out. The different dynamical regimes at increasing current are the stable emission steady state (SS), low frequency fluctuations (LFF), and coherence collapse (CC).

expected to depend on the feedback level and the injection current. These dependencies are illustrated in Fig. 9. Figure 9(a) presents the optical spectrum for very weak feedback (practically for the solitary laser). The optical spectrum for a toruslike regime at $\sigma = 20\ \mathrm{ns}^{-1}$ is shown in Fig. 9(b), and for LFF at $\sigma = 100\ \mathrm{ns}^{-1}$ in Fig. 9(c). It is evident that the linewidth is approximately proportional to the value of $\sigma$. The amount of the external modes involved into the dynamics and hence the linewidth increases also with increasing pump current. At the same time, the separation between the frequencies of the centers of mass of the spectra of the orthogonal field components becomes smaller in tendency. At that, an additional maximum near the zero frequency (the solitary laser frequency) appears in the spectra of the $E_x$ component. With further increasing of the pump current this maximum disappears again. Finally, the spectra become "bell shaped." As an example, a fairly broad spectrum of nearly Gaussian form obtained in the regime with fully developed coherence collapse is shown in Fig. 9(d).

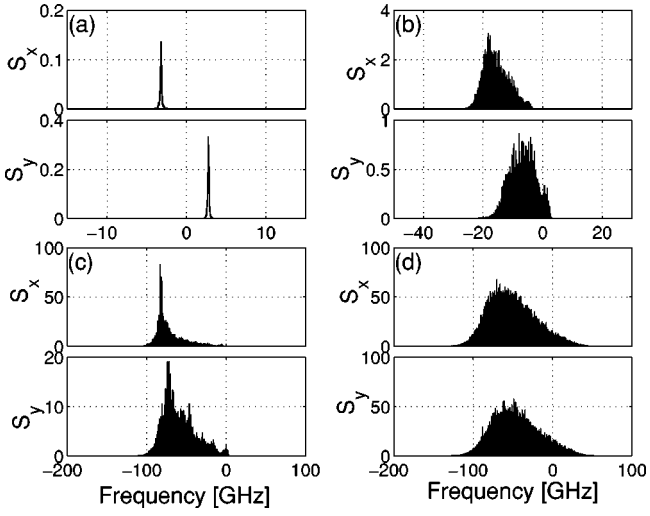


FIG. 9. Optical spectrum of the $E_x$ mode ($S_x$) and $E_y$ mode ($S_y$) at $\gamma_a = 0.04\pi\ \mathrm{ns}^{-1}$, $\sigma = 10^{-5}$ (a), $20\ \mathrm{ns}^{-1}$ (b), $100\ \mathrm{ns}^{-1}$ (c),(d), $\mu = 1$ (a)–(c), 4(d), $\beta = 10^{-5}$.

#### *4. Influence of external-cavity multiple round-trips*

As in the deterministic case, contributions of multiple round-trips in the external cavity introduce qualitative changes in the dynamics at high feedback levels. At the solitary laser threshold, instead of LFF dynamics with dropouts of the intensity in both polarization components the following sequence of dynamical behaviors is obtained, if the feedback strength is increased: stable emission in the $E_x$ component, strongly antiphased almost-periodic pulsations in both components with a period of 3 ns and with weak slow envelope, and partially antiphased LFF are obtained ($\gamma_a = 0.1\pi\ \mathrm{ns}^{-1}$). The total intensity and the total population inversion are almost constant when antiphased pulsations occur. Hence, this regime is similar to the behavior observed below the solitary laser threshold without taking into account multiple round-trips [similar to that presented in Fig. 7(c)]. It may be explained by the fact that the threshold reduction is weaker for the multiple round-trips case by a factor $1/(1+r_2r_3)$ (see also the discussion of Fig. 11). Taking into account multiple round-trips changes also the threshold current of transformation of steady states to antiphase pulsations and to LFF. Moreover, the described example shows that this can change the stability of orthogonally polarized modes giving preference to the $E_x$ component. It is worth noting that changes in behavior under multiple round-trip conditions in comparison with the single round-trip approximation in the stochastic case take place at $\sigma \geqslant 55\ \mathrm{ns}^{-1}$.

## IV. EXPERIMENTAL RESULTS AND COMPARISON TO THEORY

### A. Experimental setup

The experimental setup is described in Ref. [15]. For convenience we repeat here the most important points and hint to differences and improvements in comparison to the earlier work. The VCSELs investigated are gain-guided devices with an aperture diameter of 8 $\mu$m from EMCORE Corp. (emission wavelength in the 850 nm region). The emission is in the fundamental transverse mode up to more than two times the threshold current. The light is collected by an aspheric, antireflection coated lens. A nonpolarizing beam splitter directs a fraction (66%) of the output power onto a highly reflective mirror that forms the external cavity. From the mirror distance, the external-cavity round-trip time is calculated to be 3.25 ns (taking into account the enhancement in optical path length due to the collimator and the beam splitter cube).

The ratio of the light reflected back into the VCSEL is controlled by means of neutral density filters. The external mirror and the position of the collimation lens are adjusted to minimize the threshold of the compound system. In the absence of another criterion this is regarded as the condition of best mode-matching achievable in the experiment. It is consistent with the observation made by inspection with the eye that there is a focus of the output beam in the plane of the feedback mirror.

Low-bandwidth detectors are used to monitor the time-averaged, polarization resolved light-current characteristics. Polarization resolved time series are obtained by means of avalanche photodiodes (APD, 1.8 GHz analog bandwidth) and a digital oscilloscope (1.1 GHz analog bandwidth, sampling interval 125 ps). For spectral measurements, in some cases pin photodiodes in conjunction with an amplifier were used with a bandwidth of about 10 GHz.

For a very limited set of experiments, a digitizing oscilloscope with a bandwidth of 6 GHz (sampling interval 50 ps) was available. If the pin photodiodes are to be used for measurements with the oscilloscope, they need to be amplified. A 20 db amplification was achieved by a microwave amplifier with a bandwidth of about 20 GHz. However, these amplifiers do not transmit low frequencies so that the dc information is lost. Hence, these data were mainly used for determining the correlation properties between the polarization components. Also the signal height was only sufficient for reliable information in the coherence collapse regime, if the output of the laser had a sufficiently high amplitude.

The optical spectrum is measured with a scanning Fabry-Perot interferometer with a finesse of 200 and a free spectral range of 46 GHz.

The effective dichroism and birefringence parameters are extracted from optical or rf spectra of the free-running devices in the manner described in Refs. [30,31]. The reported results stem from two devices, which show a rather high (device 1, $\gamma_a \approx -\pi \times (4, \ldots, 4.4)\ \mathrm{ns}^{-1}$, $\gamma_p \approx \pi \times 14\ \mathrm{ns}^{-1}$) and a rather low dichroism (device 2, $\gamma_a \approx \pi \times (0.1, \ldots, 0.4)\ \mathrm{ns}^{-1}$, $\gamma_p \approx \pi \times 6\ \mathrm{ns}^{-1}$), respectively. The dichroism values can be tuned to some amount by varying the substrate temperature (the birefringence changes only by about 1 GHz for a temperature change of 50 K).

### B. LI curves

Figure 10 shows the polarization resolved (a) and the total LI curve (b) of device 2 at a feedback level of about $-10$ db. The dichroism of the device is tuned in such a way that the two polarization components are nearly on an equal footing at threshold in the free-running laser. Both modes are excited on average [18]. The width of the peaks in the optical spectrum indicates that there is still a slight preference for the high-frequency mode. However, the difference in width is at the limits of the experimental resolution ($\gamma_a \lesssim \pi \times 0.1\ \mathrm{ns}^{-1}$).

From the curves of the total power, the threshold reduction is apparent. At the solitary laser threshold ($I_{\mathrm{theor.}} = 2.98$ mA) there is indication for a kink, i.e., the slope of the LI curve changes. At higher currents the LI curve of the laser with feedback tends to the one of the solitary laser.

The polarization resolved LI curves demonstrate that for low currents (up to about 3.15 mA) the high-frequency mode is slightly dominating, whereas the low-frequency one takes over afterwards. This matches roughly the behavior encountered in the solitary laser: Both modes are excited about equally (on average) at threshold, but above threshold the high-frequency mode is continuously depleted to zero (within a current interval of about 0.25 mA) and the low-frequency mode is strongly dominating [18].

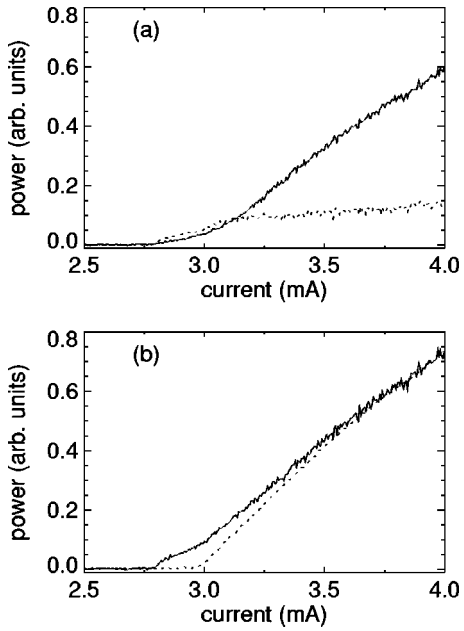


FIG. 10. Light-current characteristic for VCSEL with low dichroism in the presence of feedback: (a) polarization-resolved (dashed line, high-frequency mode corresponding to $E_y$; solid line, low-frequency mode corresponding to $E_x$); (b) total power (solid line, with feedback; dashed line, solitary laser for comparison). Parameters: device 2; $T=63\,^{\circ}\mathrm{C}$, $\gamma_a \leq \pi\times 0.1\ \mathrm{ns}^{-1}$, $\gamma_p \approx \pi\times 6\ \mathrm{ns}^{-1}$, threshold current of solitary laser $I_{\mathrm{th}}=2.98$ mA, $r_3=0.33$, threshold reduction 6.4%.

A somehow similar behavior was obtained in the simulations (see Fig. 8). In the LFF regime both modes are excited on average with approximately equal power. At increasing current, also a slight kink is observed in the total output power before the system transits into the coherence collapse regime. This kink is located at $\approx \mu = 1.1$. However, this kink is not so pronounced as that observed at the solitary laser threshold in the experiments and it appears at slightly higher injection current. At increasing current, the $E_x$ mode (i.e., the mode with lower optical frequency) is strongly dominating in the simulations. This is in accordance with the experimental results. The kink observed in the simulated LI curve at the transition from stable emission to LFF (see Fig. 8, $\mu \approx 0.9$) is not observed in the experiments. This is due to the fact that in the experiments the dynamical regime of stable emission at the reduced threshold does not appear.

### C. Threshold reduction

The threshold reduction in dependence on feedback level and substrate temperature was studied in detail in device 1. Figure 11 shows the observed threshold reduction versus the (amplitude) reflectivity of the external reflector. The normalized threshold reduction

$$\Delta\mu_{\mathrm{expt.}} := \frac{\Delta I}{I_{\mathrm{th}}} \tag{5}$$

increases monotonically with increasing feedback strength and reaches nearly 13% for the maximum value of feedback

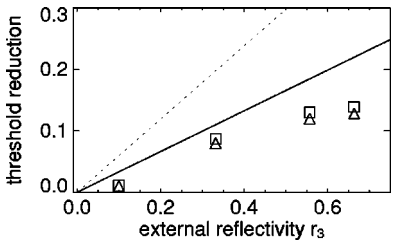


FIG. 11. Threshold reduction normalized to the threshold current in dependence on the (amplitude) reflectivity of the external reflector. Parameters: device 1; $T=20\,^{\circ}\mathrm{C}$, threshold current of solitary laser $I_{\mathrm{th}}=4.85$ mA, $\gamma_a=\pi\times 4\ \mathrm{ns}^{-1}$, $\gamma_p \approx \pi\times 14\ \mathrm{ns}^{-1}$. The lines denote the prediction of Eq. (4) in the single round-trip approximation (dashed line) and taking all round-trips into account (solid line). The value of $r_2$ is the same as that taken in Sec. II. The triangles denote experimental m easurements using Eq. (5) for normalization, the squares using Eq. (7) (see text for further explanation).

achievable in our setup ($r_3=0.67, R_3=r_3^2=0.45$). The threshold reduction depends weakly on the device temperature (span of only 0.5% in the temperature interval between $20\,^{\circ}\mathrm{C}$ and $60\,^{\circ}\mathrm{C}$) and reaches a maximum of 13.5% (for the strongest feedback) at a temperature of $43\,^{\circ}\mathrm{C}$. This point coincides with the minimum threshold condition, i.e., at this point the gain spectrum and the cavity resonance are optimally aligned.

The lines depicted in Fig. 11 denote the prediction of Eq. (4) in the single round-trip approximation (dashed line) and taking all round-trips into account (solid line). It is apparent that the feedback reduction obtained in the experiment is substantially lower than the theoretical prediction. One possible reason is imperfect mode matching, which might result from imperfect optics or a suboptimal beam quality of the VCSEL. The latter might be due to the fact that in the VCSELs under study proton implantation is used to define the active area, i.e., they are nominally gain guided and no build-in index-guiding provides a strong mode confinement.

However, it has to be kept in mind that the threshold reduction defined experimentally [Eq. (5)] and the theoretical value [Eq. (4)] cannot be compared directly, since $I=0$ denotes zero current, whereas $\mu=0$ denotes transparency (e.g., Ref. [19]). Comparing the normalized equations given here and the original equations (e.g., in Ref. [32]), the following relationship between $I$ and $\mu$ is obtained:

$$\mu \sim \left( \frac{\eta_i}{qV} I - \frac{1}{\tau_e} N_{\mathrm{tr}} \right). \tag{6}$$

Here, $N_{\mathrm{tr}}$ denotes the transparency carrier density, $q$ is the elementary charge, $\eta_i$ is the internal quantum efficiency, and $V$ is the mode volume. Hence, the threshold reduction in the ''theoretical'' scaling expressed by the experimentally measured current values is given by

$$\frac{\mu-\mu_{\mathrm{th}}}{\mu_{\mathrm{th}}} = \frac{I-I_{\mathrm{th}}}{I_{\mathrm{th}} - \dfrac{qV}{\eta_i \tau_e} N_{\mathrm{tr}}}. \tag{7}$$

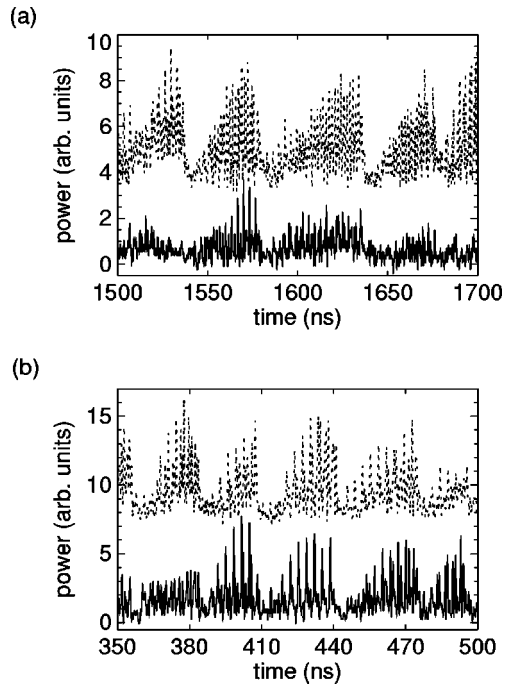


FIG. 12. Time series of the polarization resolved power (dashed line, high-frequency mode corresponding to $E_y$; solid line, low-frequency mode corresponding to $E_x$). Parameters, $T=63\,^{\circ}\mathrm{C}$, $r_3=0.33$, threshold current of solitary laser $I_{th}=2.98$ mA, threshold reduction 6.4%, $\gamma_a \lesssim \pi\times 0.1\ \mathrm{ns}^{-1}$, $\gamma_p \approx \pi\times 6\ \mathrm{ns}^{-1}$ and (a) $I=2.89$ mA ($\mu_{\mathrm{expt.}}=0.97$), (b) $I=2.98$ mA ($\mu_{\mathrm{expt.}}=1$). The time trace of the mode with the higher frequency is shifted by three vertical units (a) and seven vertical units (b).

Obviously, the correction is negligible if the transparency current $qV/(\eta_i\tau_e)N_{\mathrm{tr}}$ is much smaller than the threshold current. This is the case in lasers with a low finesse cavity which often holds for edge-emitting lasers. However, in a VCSEL the correction might be substantial due to the high-quality factor of the cavity. Taking the value $\tau_e=1$ ns assumed before in the simulations, and literature values from Ref. [32] ($\eta_i=0.8$, $N_{\mathrm{tr}}=1.8\times 10^{18}\ \mathrm{cm}^{-3}$ for $GaAs/Al_{0.2}Ga_{0.8}As$ quantum wells of 8 nm width, $V=1.056\times 10^{-12}\ \mathrm{cm}^3$ for a laser with an effective cavity length of 1.17 $\mu$m, radius of 4 $\mu$m, and a longitudinal confinement factor of 0.021), the experimentally measured values can be rescaled. The resulting data points are depicted as squares in Fig. 11. It is apparent that the agreement between experiment and theory can be improved by taking into account a finite value of the transparency current. However, quantitative considerations remain difficult, since many of the parameters used above might differ in our device and a direct measurement is not possible with the methods at our hand. Hence, we will use Fig. 11 only as a rough guideline for identifying the feedback level appropriate for comparing experimental and simulated time series.

### D. Low dichroism case: Dynamics

In Fig. 12, typical polarization resolved time series of the dynamics obtained in the LFF regime for a laser with a low dichroism (device 2) are displayed. As discussed in Sect. IV B in conjunction with the LI curves, both polarization components are excited on average. However, they show dynamics on two different time scales. The output consists of pulses whose amplitude is modulated by a low-frequency envelope. As it is evident from the figure, the low-frequency envelope consists of power drops followed by a slow recovery. The characteristic features of this time trace resemble the shape of typical LFF occurring in edge-emitting semiconductor lasers (e.g., Refs. [33], and references therein). The power builds up on a time scale of some tens of nanoseconds and then drops suddenly. The underlying structure of this slow dynamics consists of peaks of increasing height which are separated by the external-cavity round-trip time ($\approx 3.3$ ns).

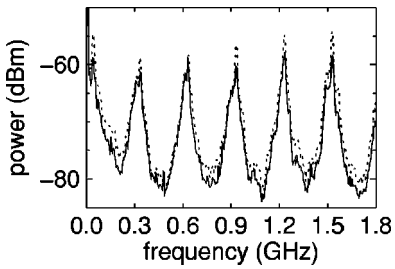


FIG. 13. Polarization resolved rf spectra in logarithmic scale (dashed line, $E_y$; solid line, $E_x$). Parameters as in Fig. 12(b).

The rf spectrum shows peaks at multiples of the external-cavity frequency and a strong peak around 30 MHz corresponding to the LFF (Fig. 13), which is an indication for rather periodic dynamics on the slow timescale. The rf spectra are virtually identical for the two components except for the fact that the $E_x$ component has a slightly higher amplitude.

In between the large-amplitude pulses separated by the external-cavity round-trip time, peaks of lower amplitude exist. The separation of the latter ones is less than 1 ns. The corresponding frequency is at the limit of the bandwidth of our experimental setup, thus we cannot give definite information on their exact temporal development. The rf spectra (Fig. 13) clearly demonstrate that there is dynamics on time scales below 1 ns.

A detailed experimental investigation of the frequency and strength of the LFF in dependence on the injection current is shown in Fig. 14. The frequency of the LFF increases approximately linearly in their existence region [from 8 to 50 MHz, see Fig. 14(a)]. As depicted in Fig. 14(b), the amplitude of the LFF peaks reaches a maximum around the threshold of the solitary laser. Afterwards it decreases again. At the same time dropouts become more frequent until single events cannot be distinguished anymore. Here, the laser reaches the regime of coherence collapse. This regime is discussed further in Sec. IV E.

The observed behavior in the LFF regime close to the solitary laser threshold disagrees strongly with the predictions of a quasiperiodic locked state for a deterministic system (Figs. 1 and 2) but matches well the prediction of the numerical simulations including noise in many respects. The results presented in Fig. 12(b) need to be compared with the

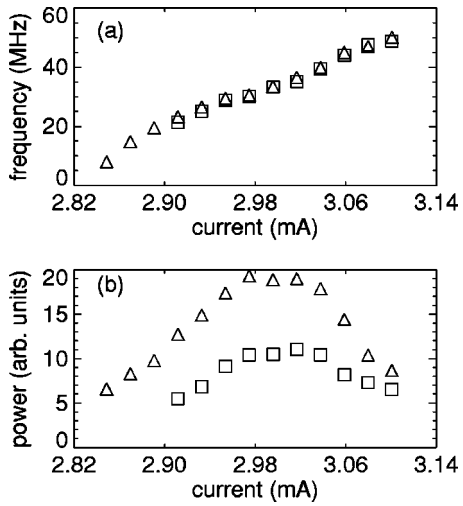


FIG. 14. Frequency (a) and amplitude (b) of LFF peak in power spectrum in dependence on current. Triangles denote the $E_y$ mode; squares denote the $E_x$ mode. Parameters are as in Fig. 12.

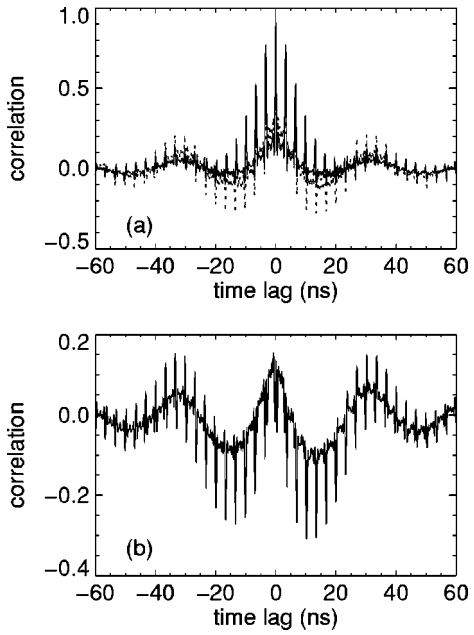


FIG. 15. (a) Autocorrelation functions (dashed line, high-frequency mode; solid line, low-frequency mode) and (b) cross-correlation function of the two polarization components. The correlation functions are calculated for a 50-$\mu$s-long time series via the Wiener-Khintchin theorem. The times series was divided in 50 segments and the resulting correlation functions were averaged [36]. Parameters are as in Fig. 12(b).

numerically obtained ones presented in Fig. 6, which are obtained for comparable parameters (see Sec. IV C for a discussion of the feedback strength). In the experiment and in the simulations, both polarization components are excited on average. The one favored by the dichroism of the solitary laser has a slightly higher amplitude (below and around the solitary laser threshold). Both polarization modes undergo LFF with an asymmetric shape, i.e., a sudden power drop is followed by a slow recovery. The dropout events occur simultaneously in both components. The frequency of the LFF increases in both cases with current until single events cannot be distinguished anymore and the regime of coherence collapse is reached. However, in tendency the frequency is lower in simulations than in the experiment.

The tendency of an increase of the frequency of the LFF cycles with increasing current is also found in the simulations. Depending on the parameters, this frequency is on average about a factor 3–4 smaller in the simulations. Also, the frequency of the cycles is of less regularity than in the experiment. We should note, however, that the frequency of the LFF cycles in the experiment is close to the slow frequency of the torus observed in the simulations. The question of the relationship between the period of the LFF cycles in the experiments and in the simulations requires further investigations.

LFF characterized by the simultaneous dropout of both polarization components were first predicted in Ref. [14] for a VCSEL with isotropic feedback and a small dichroism (investigated value of $\gamma_a = 0.1 \times 10^9\ \mathrm{s}^{-1}$). They were also found in Ref. [13] and termed ''type-I LFF.'' Both papers report the occurrence of this kind of LFF only for injection currents above and at the threshold of the solitary laser, whereas we observed them in the experiment also below the solitary laser threshold. With a value of the linewidth enhancement factor of $\alpha = 3$ (as used in Refs. [13,14]) we were not able to obtain LFF below the solitary laser threshold in numerical simulations even if noise was included. Also the dropouts in the LFF above threshold were not very pronounced for this choice of $\alpha$.

Only, if the linewidth enhancement factor was increased to about 5, this became a robust feature of the dynamics. This numerical observation motivated the choice of $\alpha = 5$ in the simulations presented above, although this value is often regarded to be quite high for a quantum well device. Many authors obtain values of $\alpha = 2.5, \ldots, 3$ (e.g., Refs. [30,34]), however also values of 5 were measured [35]. Hence, we do not consider the value used as being unreasonable as long as we do not have an independent measure. We remark that also the quasiperiodic locked state occurs only for $\alpha \gtrsim 5$. This matches the reports of Refs. [23,25] on edge-emitting lasers, in which a value of $\alpha = 6$ is used. It is tempting to conjecture that the occurrence of noise-induced LFF below the solitary laser threshold is somehow linked to the existence of the locked state, but we cannot say anything definite at the present stage of the investigations.

On the fast time scales, the dynamics is characterized by pulsing on the external-cavity round-trip scale ($\approx 3.3$ ns) and a nanosecond and subnanosecond scale (see Fig. 12). This is true both in the experiment and in the simulations. It is also well known for edge-emitting lasers [20,22,25,26] and was predicted before for VCSELs with isotropic feedback [4,13,14]. The previous experimental investigations in Ref. [4] gave only indirect evidence in the spectral domain.

For a more detailed analysis, Fig. 15(a) displays the autocorrelation function of the time series of the two polarizations. It is apparent that the external-cavity round-trip time is the most prominent feature. The slower modulation corresponds to the LFF cycle. It is apparent that some correlation on the round-trip time scale survives for more than one LFF cycle. In an autocorrelation function calculated over a large

time series (thus averaging over many LFF events), there are no pronounced features on a nanosecond or subnanosecond time scale indicating that the pulsing on the very fast scales is quite irregular and different from LFF event to LFF event (some oscillations survive if the autocorrelation function is calculated over only one or a few LFF cycles). This meets observations in edge-emitting lasers [22].

The correlation properties between the two polarization components are also of obvious interest. The cross-correlation function [Fig. 15(b)] is also dominated by the external cavity and the LFF time scale. The fact that the overall correlation is positive around time lag zero reflects the fact that the average evolves rather synchronously in both polarization components during a LFF event. The recurrence of the correlation at a time lag of $\pm 32$ ns reflects that the average behavior in subsequent LFF is similar. Superimposed on this slowly varying envelope are negative spikes indicating anticorrelation. Anticorrelation is in accordance with the impression got by visual inspection of the time series. A closer inspection shows that the negative spikes around time lag zero have a substructure indicating a more complicated behavior. Indeed, looking through the time series, one can find examples of other correlation behaviors. Examples are shown in Fig. 16.

To start with, Fig. 16(a) shows the enlargement of a part of Fig. 12(b). In the time window between 8 and 20 ns both polarization components are characterized by a sequence of pulses separated by $\tau$, which are interleaved. In addition, low-amplitude pulses exist and occur partly at the same time as a large-amplitude pulse in the other polarization component, but can be also displaced. Between 20 and 30 ns two pulses of the high-frequency mode occur within a 3.3 ns interval between two pulses of the low-frequency mode.

In Fig. 16(b) more or less every pulse in one mode is accompanied by a pulse in the other mode, but the heights show a strong anticorrelation. A coincidence between most pulses in the two polarization components is also apparent in Fig. 16(c). Now the pulses are even of nearly the same height so that one should speak of a rather synchronized behavior.

Finally, in Fig. 16(d) the behavior changes over the duration of the LFF cycle. While the pulses are correlated at the beginning (0–15 ns), they are anticorrelated at later times (15–43 ns). The two last pulses (45–48 ns) are again correlated.

Evidence for anticorrelated as well as correlated behavior can be obtained also from the cross-power spectrum,

$$C(f)=\tilde{I}_x(f)\tilde{I}_y^*(f), \tag{8}$$

where the tilde denotes the Fourier transform. In this unnormalized form, a positive value denotes correlation, a negative one denotes anticorrelation. After a normalization by $\sqrt{|\tilde{I}_x(f)|^2|\tilde{I}_y(f)|^2}$ one obtains directly a correlation factor between $-1$ and 1 in dependence of frequency. In Fig. 17, the unnormalized cross-power spectrum is shown since we want to compare it with the power spectra of the individual polarization components.

One prominent feature in Fig. 17(a) is the peak around 30 MHz. It is present in both polarization components and represents the LFF dynamics. The cross-power spectrum has a positive value at this frequency, indicating correlation (about 0.8 in normalized units). This reflects the synchronous LFF dynamics in both polarizations. For even lower frequencies, there is a low-frequency shoulder which might be also partly due to technical noise. This is anticorrelated in the polarization components. Anticorrelation at low frequencies is a very well-known feature in free-running VCSELs (e.g., Refs. [18,37–39]).

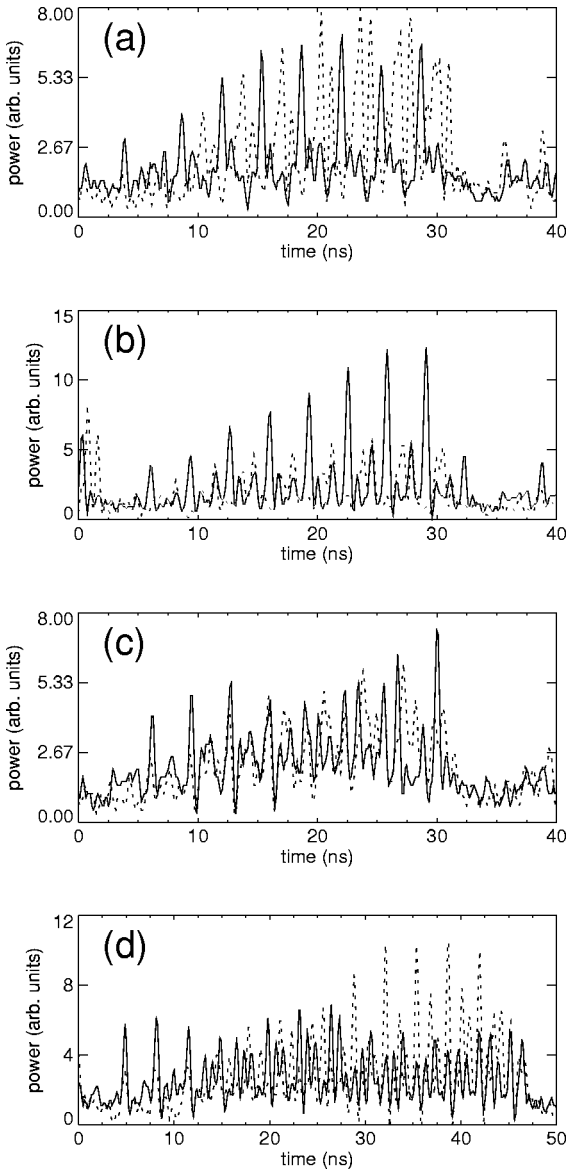


FIG. 16. Examples of single LFF events out of a time series of 50 $\mu$s (dashed line, high-frequency mode; solid line, low-frequency mode). Parameters are as in Fig. 12(b). (b) and (c) show LFF events following each other.

The power spectrum in the vicinity of the external-cavity round-trip time displays actually a two-peaked structure [see the central structure in Fig. 17(a) and the enlargement in Fig. 17(b)]. This is also present in Fig. 13 but is not so obvious because of the logarithmic scale used there. The broader, left peak is centered around 0.305 GHz, which is the inverse of the external-cavity round-trip time of 3.25 ns. The sharper

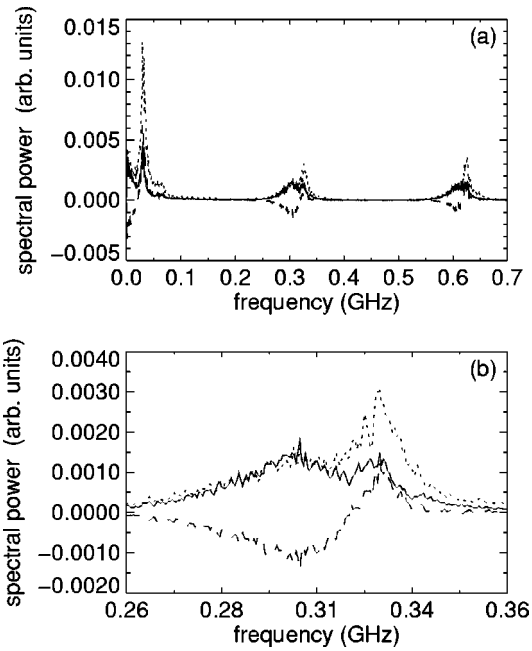


FIG. 17. Power spectrum of polarization components (short-dashed line, high-frequency mode; solid line, low-frequency mode) and cross-power spectrum (dashed line). (b) is an expansion of (a) around the external-cavity round-trip frequency. The power spectrum is calculated from a 50-$\mu$s-long time series. The times series was divided in 50 segments and the resulting power spectra were averaged [36]. Parameters are as in Fig. 12(b).

other peak is centered around 0.327 GHz (its position depends slightly on the current level). At the frequency of the external-cavity round-trip, the dynamics is anticorrelated (correlation factor about $-0.8$), whereas it is correlated at the other peak (correlation factor about 0.7). At the present stage of the investigations, we cannot give a further interpretation of this behavior. We remark that a splitting of the peaks at the external-cavity round-trip time was observed also in Ref. [4] and was conjectured to result from a mixing of the external-cavity round-trip frequency with a low-frequency oscillation. In our case, the splitting has a similar order of magnitude as the frequency of the LFF peak (about 5–10 MHz smaller) and the same current dependence. This gives some support to the idea that the double structure results from a nonlinear mixing process of the external round-trip frequency and the LFF frequency. A splitting of the peaks at the external-cavity round-trip frequency is also known from edge-emitting lasers with feedback [40,41]. In Ref. [40] it was explained as being due to correlations between different external-cavity modes with slightly different losses. The relationship between the two proposed explanations remains open at the moment.

A double-peak-like structure at the external-cavity frequency is also observed in the cross-spectral densities of the simulated time traces (Fig. 18). The visibility of the double peak in the power spectra of the polarization modes depends on the feedback strength $\sigma$. Also in the simulations, the peak at the external-cavity resonance shows anticorrelation and the shifted peak correlation, respectively. However, the cross-correlation function of the modes in the time domain

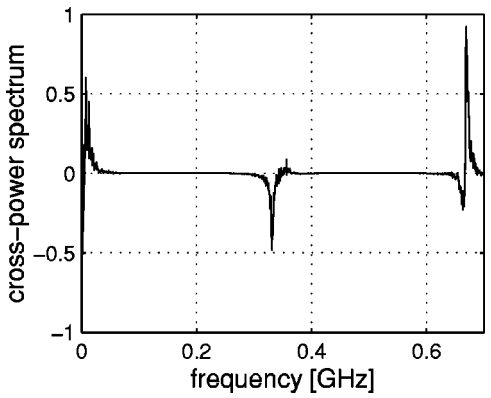


FIG. 18. Cross-power spectrum. Parameters are as in Fig. 6.

shows correlated dynamics at the external-cavity round-trip time and a strong correlation (about 0.5 in normalized values) at zero time lag.

The correlation behavior between different longitudinal modes was heavily debated in edge-emitting semiconductor lasers with feedback [26,42–44] and has possible implications for the role of multimode emission in creating a LFF event [26]. The possibility of in-phase and out-of-phase dynamics within a single LFF period was obtained before in numerical simulations of a multimode extension of the Lang-Kobayashi equations for external-cavity edge-emitting laser diodes [44], and, very recently, for the polarization modes in a VCSEL with feedback [13]. Experimentally, a change of the correlation behavior was indeed observed in multimode edge-emitting lasers [26]; however, the synchronized regime was found in a small time slot just before a LFF event.

Our numerical results agree quite well with the results of Ref. [44] for edge-emitting lasers and Ref. [13] for VCSELs. Due to the variety of behaviors observed in the experiment, it is not straightforward to compare the experimentally observed correlation properties with the results of the numerical simulations. The behavior found in Fig. 16(b) (synchronous pulses with an antiphase behavior in their height) agrees most closely to the typical behavior found in the simulations. However, antiphase behavior on the time scale of the external cavity appears to play a somehow more pronounced role in the experiment than in the simulations. We conclude that from an experimental point of view we cannot give a definite answer on the correlation properties within a single LFF cycle but have to restrict to the features apparent in the long time average discussed above. From a statistical point of view, the long time average indicates a preference for anti-correlated dynamics at the external-cavity round trip frequency [see Figs. 15(b) and 17(b)]. This is in contrast to the correlation properties of the dynamics in the simulations, where on the long time average strong correlation is obtained. Probably, stochastic effects are very important in the experiment.

Also the question, whether very close to threshold purely antiphase oscillations at the external-cavity round-trip time (without low-frequency component) exist, remains open from the experimental point of view. Directly at the reduced lasing threshold the laser output power is already fluctuating, but it is difficult to recognize a characteristic structure. The

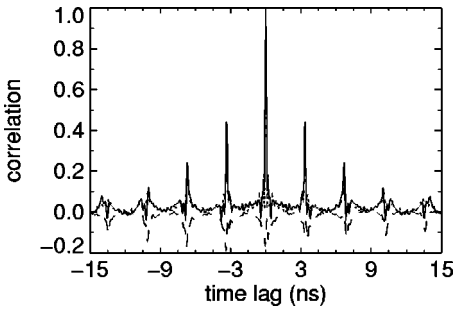


FIG. 19. Autocorrelation (short-dashed line, high-frequency mode; solid line, low-frequency mode) and cross correlation (short-dashed line) of the time series of polarization components. The correlation function is calculated from a 50 $\mu$s (bandwidth 6 GHz) long time series divided into 50 segments. Parameters are comparable to those in Fig. 12, but $r_3=0.67$, threshold current of solitary laser $I_{\mathrm{th}}=2.99$ mA, threshold reduction 10.6%, $I=3.4$ mA ($\mu_{\mathrm{expt.}}=1.14$).

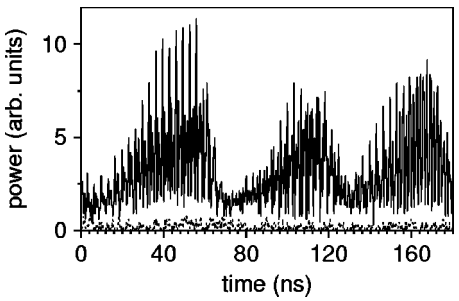


FIG. 20. Time series of the polarization resolved power for a VCSEL with a large dichroism (device 1; dashed line, high-frequency mode; solid line, low-frequency mode). Parameters, $T=20\,^{\circ}\mathrm{C}$, $r_3=0.33$, threshold current of solitary laser $I_{\mathrm{th}}=4.85$ mA, threshold reduction 8%, $\gamma_a=-\pi\times 4\ \mathrm{ns}^{-1}$, $\gamma_p\approx\pi\times 14\ \mathrm{ns}^{-1}$, and $I=4.59$ mA ($\mu_{\mathrm{expt.}}=0.95$).

amplitude of the fluctuations grows continuously, if the current is increased. At about 2% above threshold, the LFF structure becomes discernible. Antiphase oscillations below the solitary laser threshold were also obtained in a different VCSEL model [4]. Also in that case, no clear experimental proof could be given.

### E. Transition to coherence collapse

In the coherence collapse regime, the experimentally observed time series appears to be quite irregular and oscillates about a nonzero mean (see Fig. 5 of Ref. [15]). However, one needs to be aware of the fact that most of the dynamics left the bandwidth of the APDs. Measurements of the rf spectrum with the pin photodiodes show a broad spectrum with superimposed peaks at multiples of the external-cavity round-trip frequency. Far enough beyond threshold, the spectrum extends to 10 GHz (and possibly above). The autocorrelation and cross-correlation functions of the two polarization components measured with a bandwidth of 6 GHz are shown in Fig. 19. Clearly, the external-cavity round-trip time of about 3.3 ns is still a dominant feature of the dynamics. In the time series, irregular oscillations on the sub-nanosecond scale are present which, however, do not appear in autocorrelation functions calculated over large time intervals. This indicates that the dynamics on the faster time scales are highly irregular. This meets observations in edge-emitting laser obtained by streak-camera measurements [22,26]. The prevalence of the external-cavity round-trip time even in the coherence-collapse regime was also noted in edge-emitting lasers [41]. The dynamics of the two polarization components are now anticorrelated at the external-cavity round-trip frequency (Fig. 19). The strength of the anticorrelation increases for increasing current and reaches values less than $-0.9$ in fully developed coherence collapse.

In the simulations, the dynamics are correlated at the external-cavity round-trip frequency in the regime of coherence collapse. Since in the experiments the dynamics are clearly anticorrelated also in this dynamical regime, one can speak of a clear discrepancy regarding the correlation properties between experiments and simulations.

We remark that coherence collapse in VCSELs with feedback was observed by purely spectral measurements before [1,45], but these works did not consider polarization properties. On the other hand, in Ref. [4] a transition to a stable state (and no coherence collapse) was observed in experiments, if the current was increased above the LFF regime, whereas the theoretical results presented in Ref. [4] predicted indeed the transition to a coherence collapse regime. Hence, we consider our measurements presented in Ref. [15] and here in connection with the theoretical treatment as helping to clarify the situation. Indeed, coherence collapse appears to be a robust feature of the dynamics of VCSELs with feedback.

### F. Influence of dichroism

In Fig. 20, a time series obtained with a VCSEL with a large dichroism is shown. The dominant polarization mode displays LFF behavior, whereas the power in the polarization corresponding to the mode with higher optical frequency remains on the spontaneous emission level. The time-averaged optical spectrum shows one lasing mode and filtered spontaneous emission around the frequency of the nonlasing mode. The nonlasing peak is not amplified with respect to the case without feedback.

The LFF exist in a current range from slightly above the reduced threshold of the compound system to about 0.1 mA beyond the threshold of the solitary laser. Above that value, coherence collapse is encountered. The properties of the LFF do not seem to deviate from those in the low dichroism case.

In the simulations an increase of the dichroism between the two polarization components increases the difference between the average amplitudes of the polarization components. Thus, for the case of a very strong dichroism ($|\gamma_a|=4\pi\ \mathrm{ns}^{-1}$), the intensity of the $E_y$ component, which is favored by dichroism, is more than $5\times 10^4$ times larger than the intensity of the $E_x$ component even if spontaneous emission noise is included. In the experiment, it cannot be clearly said whether the weak mode exhibits fluctuations on an intensity level that is several orders of magnitude smaller than the intensity of the dominating mode, since this span is beyond the dynamic range of the measurement system.

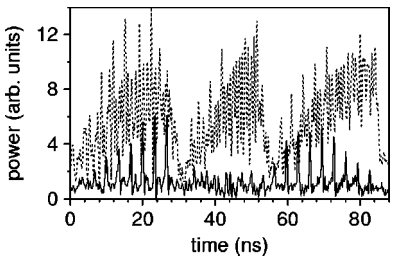


FIG. 21. Time series of the polarization resolved power for a VCSEL with an intermediate dichroism (device 2; dashed line, high-frequency mode; solid line, low-frequency mode). Parameters, $T=19\,^{\circ}\mathrm{C}$, $r_3=0.33$, threshold current of solitary laser $I_{\mathrm{th}}=3.6$ mA, threshold reduction 8%, $\gamma_a=\pi\times 0.4\ \mathrm{ns}^{-1}$, $\gamma_p\approx\pi\times 6\ \mathrm{ns}^{-1}$, and $I=3.64$ mA ($\mu_{\mathrm{expt.}}=1.01$).

With noise, the system is in a state of stable emission of the $E_y$ mode at the reduced threshold, whereas the $E_x$ component remains on the noise level. At increasing current, but still below the solitary laser threshold, the dynamics change to LFF as in the case of small dichroism. After an dropout event, also the $E_x$ mode is excited and its intensity increases and reaches a maximum when the recovery process of the dominating $E_y$ mode is finished. After that, the $E_x$ mode is depleted and remains off until the next dropout event. In the deterministic case, the dominating mode exhibits toruslike dynamics and the weak mode remains off all the time (even in the low-power periods of the dominating mode). Depending on the magnitude of $\sigma$ and $\mu$ the torus is disturbed with a tendency to an asymmetric— LFF-like—shape. These numerical observations indicate that neither the toruslike nor the LFF-like dynamics depend on the excitation of a second mode.

For an intermediate value of the dichroism ($\gamma_a=\pi\times 0.4\ \mathrm{ns}^{-1}$), the experimental scenario is as follows (see Fig. 21): We observe LFF for the dominating mode, which is in this case the one with higher optical frequency. (This is also the lasing mode of the solitary laser.) The dynamics of the mode that is disfavored by the dichroism are different for different LFF cycles of the dominating mode. In many cycles the power of the weaker mode remains on (or very close to) the spontaneous emission level. In some cycles also the weaker mode shows LFF, but with a smaller amplitude than in the dominating mode. In these cases dropouts are synchronous in the two polarization components. In the rest of the cycles the weak mode also starts with pulsations, but these pulsations die out before the LFF cycle of the dominant mode is completed, i.e., the slow dynamics become antiphased towards the end of the LFF cycle. The part of the time series displayed in Fig. 21 has been selected to demonstrate all of the three behaviors described above.

For $\gamma_a=0.4\pi\ \mathrm{ns}^{-1}$, which matches the value of the experimental dichroism in Fig. 21, we observe in simulations with noise a behavior of LFF in both components with comparable amplitude of the pulsations similar to the results obtained in Fig. 6.

For the case of $\gamma_a=\pi\ \mathrm{ns}^{-1}$, the relative ratio between the two polarization components is in between the values found for the limiting cases discussed above. In the stochastic case, we observe LFF of the dominant mode and a behavior of the weaker mode that matches the experimental dynamics displayed in Fig. 21. For further increasing dichroism, the dynamics tend to a behavior that is dominated by simultaneous increases of the mode after a dropout and a depletion of the $E_x$ mode before the end of the LFF cycle. The larger the dichroism, the closer the point of depletion of the $E_x$ mode moves to the beginning of a LFF cycle, until the situation reported above for $\gamma_a=4\pi\ \mathrm{ns}^{-1}$ is encountered. Obviously, this type of behavior is common for semiconductor lasers with gain anisotropies of the modes participating in the dynamics, e.g., also VCSELs with polarized feedback [10] and edge-emitting lasers with frequency-selective feedback [11,12,46].

The appearance of a burst in the normally suppressed polarization component at a LFF event in the dominant one roughly matches the experimental and numerical observations in Ref. [4]. LFF of this kind were also obtained numerically in Ref. [13] and termed ''type-II LFF.'' In the latter paper, it is also reported that one can move between type-I LFF (synchronous dropouts) and type-II LFF (dropouts and bursts) by changing the anisotropies of the free-running laser. However, the type-I LFF reported in Ref. [13] were obtained for the case of elliptical polarization, i.e., the polarization modes were locked to a single frequency. This is not the case in our experiments and simulations showing type-I LFF. This difference may be due to the fact that the choice of parameters leading to type-I LFF in Ref. [13] is likely to favor elliptically polarized states also in the solitary laser.

## V. CONCLUSION

In this work, low-frequency fluctuations and polarization dynamics in VCSELs with external isotropic feedback were investigated numerically. The analysis was done in the framework of the spin-flip model modified by delayed feedback terms. The dynamics is characterized by short pulses emitted at the external-cavity round-trip frequency and multiples of it and a low-frequency envelope. On the long time scales, spontaneous emission noise proved to be crucial in exciting a train of sudden, asymmetric power drops in the vicinity of the solitary laser threshold. The shape of this dropouts matches the shape known from the low-frequency fluctuations (LFF) in edge-emitting semiconductor lasers. The polarization dynamics can exhibit simultaneous LFF, LFF of one mode with short excitation of the other mode after a dropout of the dominant mode, and intermediate scenarios. The average intensity ratio between the two polarization components and the occurrence of the above-mentioned scenarios was shown to depend on the dichroism of the device.

The theoretical results have been shown to match qualitatively well the experimental observations for different values of the dichroism. This suggests that a VCSEL with feedback is a suitable system to study and compare the properties of LFF in a two-mode and in a single-mode situation. Furthermore, both in experiments and simulations a transition from LFF to coherence collapse was observed for increasing injection current. However, the clarification of the discrepancy

of the correlation properties of the polarization components is an important subject for future studies.

The agreement found between experiment and theory for the single-round-trip case and for multiple round-trips in the external cavity with feedback strengths less than $\sigma = 50, \ldots, 60\ \mathrm{ns}^{-1}$, where the dynamics are qualitatively unchanged, indicates that in the experiments the *effective* level of feedback was in the regime of the single round-trip approximation.

## ACKNOWLEDGMENTS

This work was supported by the Deutsche Forschungsgemeinschaft. Some of the experimental time traces were obtained in collaboration with H. Bohnet.

[1] Y.C. Chung and Y.H. Lee, IEEE Photonics Technol. Lett. **3**, 597 (1991).
[2] J.W. Bae, H. Temkin, S.E. Swirhun, W.E. Quinn, P. Brusenbach, C. Parsons, M. Kim, and T. Uchida, Appl. Phys. Lett. **63**, 1480 (1993).
[3] S. Jiang, M. Dagenais, and R.A. Morgan, IEEE Photonics Technol. Lett. **7**, 739 (1995).
[4] M. Giudici, S. Balle, T. Ackemann, S. Barland, and J.R. Tredicce, J. Opt. Soc. Am. B **16**, 2114 (1999).
[5] F. Robert, P. Besnard, M.L. Chares, and G.M. Stephan, Opt. Quantum Electron. **27**, 805 (1995).
[6] S. Jiang, Z. Pan, M. Dagenais, R. Morgan, and K. Kojima, Appl. Phys. Lett. **63**, 3545 (1993).
[7] N. Badr, I.H. Whits, M.R.T. Tan, Y.M. Houng, and S.Y. Wang, Electron. Lett. **30**, 1227 (1994).
[8] P. Besnard, F. Robert, M.L. Charès, and G.M. Stéphan, Phys. Rev. A **56**, 3191 (1997).
[9] N.A. Loiko, A.V. Naumenko, and N.B. Abraham, Quantum Semiclassic. Opt. **10**, 125 (1998).
[10] N.A. Loiko, A.V. Naumenko, and N.B. Abraham, J. Opt. B: Quantum Semiclassical Opt. **3**, S100 (2001).
[11] M. Giudici, L. Giuggioli, C. Green, and J.R. Tredicce, Chaos, Solitons Fractals **10**, 811 (1999).
[12] F. Rogister, M. Sciamanna, O. Deparis, P. Megret, and M. Blondel, Phys. Rev. A **65**, 015602 (2002).
[13] M. Sciamanna, C. Masoller, N.B. Abraham, F. Rogister, P. Mégret, and M. Blondel, J. Opt. Soc. Am. B **20**, 37 (2003).
[14] C. Masoller and N.B. Abraham, Phys. Rev. A **59**, 3021 (1999).
[15] M. Sondermann, H. Bohnet, and T. Ackemann, Phys. Rev. A **67**, 021802 (2003).
[16] M.S. Miguel, Q. Feng, and J.V. Moloney, Phys. Rev. A **52**, 1728 (1995).
[17] R. Lang and K. Kobayashi, IEEE J. Quantum Electron. **16**, 347 (1980).
[18] M. Sondermann, M. Weinkath, T. Ackemann, J. Mulet, and S. Balle, Phys. Rev. A (to be published).
[19] J. Martín-Regalado, F. Prati, M.S. Miguel, and N.B. Abraham, IEEE J. Quantum Electron. **33**, 765 (1997).
[20] S.P. Hegarty, G. Huyet, P. Porta, and J.G. McInerney, Opt. Lett. **23**, 1206 (1998).
[21] C. Risch and C. Voumard, J. Appl. Phys. **48**, 2083 (1977).
[22] I. Fischer, G.H.M.v. Tartwijk, A.M. Levine, W. Elsässer, E. Göbel, and D. Lenstra, Phys. Rev. Lett. **76**, 220 (1996).
[23] R.L. Davidchack, Y.-C. Lai, A. Gavrielides, and V. Kovanis, Phys. Rev. E **63**, 056206 (2001).
[24] P. Besnard, B. Meziane, and G.M. Stéphan, IEEE J. Quantum Electron. **29**, 1271 (1993).
[25] A. Gavrielides, T.C. Newell, V. Kovanis, R.G. Harrison, N. Swanston, D. Yu, and W. Lu, Phys. Rev. A **60**, 1577 (1999).
[26] G. Vaschenko, M. Giudici, J.J. Rocca, C.S. Menoni, J.R. Tredicce, and S. Balle, Phys. Rev. Lett. **81**, 5536 (1998).
[27] I. Wallace, D. Yu, R.G. Harrison, and A. Gavrielides, J. Opt. B: Quantum Semiclassical Opt. **2**, 447 (2000).
[28] L. Gammaitoni, P. Hanggi, P. Jung, and F. Marchesoni, Rev. Mod. Phys. **70**, 223 (1998).
[29] G.H.M.v. Tartwijk, A.M. Levine, and D. Lenstra, IEEE J. Sel. Top. Quantum Electron. **1**, 466 (1995).
[30] M.P.v. Exter, M.B. Willemsen, and J.P. Woerdman, Phys. Rev. A **58**, 4191 (1998).
[31] T. Ackemann and M. Sondermann, Proc. SPIE **4286**, 44 (2001).
[32] L.A. Coldren and S.W. Corzine, *Diode Lasers and Photonic Integrated Circuits* (Wiley, New York, 1995).
[33] *Nonlinear Laser Dynamics: Concepts, Mathematics, Physics, and Applications International Spring School*, edited by B. Krauskopf and D. Lenstra, AIP Conf. Proc. No. 548 (AIP, Melville, NY, 2000).
[34] H. Li, IEEE Photonics Technol. Lett. **8**, 1594 (1996).
[35] W. Schmid, C. Jung, B. Weigl, G. Reiner, R. Michalzik, and K.J. Ebeling, IEEE Photonics Technol. Lett. **8**, 1288 (1996).
[36] W.H. Press, B. Flannery, S. Teukolsky, and W. Vettering, *Numerical Recipes, The Art of Scientific Computing* (Cambridge University Press, Cambridge, 1992).
[37] G. Giacomelli, F. Marin, M. Gabrysch, K.H. Gulden, and M. Moser, Opt. Commun. **146**, 136 (1998).
[38] J. Mulet, C. Mirasso, and M. San Miguel, Phys. Rev. A **64**, 023817 (2001).
[39] J. Kaiser, C. Degen, and W. Elsässer, J. Opt. Soc. Am. B **19**, 672 (2002).
[40] M.P.v. Exter, R.F.M. Hendriks, J.P. Woerdman, and C.J.v. Poel, Opt. Commun. **110**, 137 (1994).
[41] M. Giudici, C. Green, G. Giacomelli, U. Nespolo, and J.R. Tredicce, Phys. Rev. E **55**, 6414 (1997).
[42] D.W. Sukow, T. Heil, I. Fischer, A. Gavrielides, A. Hohl-AbiChedid, and W. Elsäßer, Phys. Rev. A **60**, 667 (1999).
[43] E.A. Viktorov and P. Mandel, Phys. Rev. Lett. **85**, 3157 (2000).
[44] F. Rogister, P. Megret, O. Deparis, and M. Blondel, Phys. Rev. A **62**, 061803 (2000).
[45] C.H.L. Quay, I.Z. Maxwell, and J.A. Hudgings, J. Appl. Phys. **90**, 5856 (2001).
[46] G. Huyet, J.K. White, A.J. Kent, S.P. Hegarty, J.V. Moloney, and J.G. McInerney, Phys. Rev. A **60**, 1534 (1999).